Wear 317 (2014) 201–212

Contents lists available at ScienceDirect

Wear

journal homepage: www.elsevier.com/locate/wear

Tribological and mechanical behavior of multilayer Cu/SiC + Gr hybrid composites for brake friction material applications

T. Ram Prabhu [a,*], V.K. Varma [a], Srikanth Vedantam [b]

[a] Centre for Military Airworthiness and Certification, Marathalli Colony Post, Bangalore, India
[b] Department of Engineering Design, Indian Institute of Technology, Madras, India

ARTICLE INFO

Article history:
Received 28 April 2014
Received in revised form
4 June 2014
Accepted 7 June 2014
Available online 16 June 2014

Keywords:
Wear testing
Surface analysis
Brakes/clutches
Metal–matrix composite
Optical microscopy

ABSTRACT

In this paper, we study the wear resistance of multi-layered composites of Cu/SiC + Gr hybrid composites prepared by layer compaction and pressure sintering. The tribological behavior and wear resistance of the composites were evaluated at a range of sliding speeds (5, 10, 30 and 35 m/s) in a laboratory scale inertia brake dynamometer for brake friction material applications. The wear surface morphology and mechanisms were studied using scanning electron microscopy (SEM), XRD, and stereoscopy. The microstructure of the composites was also characterized using SEM and optical microscopy and the mechanical response in compression and flexure was evaluated. The results of these tests indicate that the density, wear resistance, braking behavior and mechanical response can be significantly improved by the presence of a layer of copper away from the sliding surface. The presence of the layer also improved friction and wear resistance significantly. The formation of mechanically mixed tribolayer and oxides (Fe_3O_4) reduced the wear rate and stabilized the friction coefficient at 30 and 35 m/s. Finally, crack deflection and branching at the interface between the composite and Cu layers improved the flexural strength of the layered composites. The fractography analysis indicates a quasi-cleavage intergranular fracture in the composite layer and a purely ductile fracture in the Cu layer.

1. Introduction

The potential use of Cu/SiC composites in frictional applications such as brakes and clutches has not yet been widely explored in spite of their wide use in thermal and electrical applications [1–3]. Good friction materials generally possess a high friction coefficient, high wear resistance, high thermal conductivity and thermo-mechanical stability, high toughness and a low coefficient of thermal expansion (CTE). These properties can be obtained in Cu/SiC metal matrix composite as noted by [4] at low load (15 N) and speed (1 m/s) conditions. Similarly, other studies on Cu/SiC or Cu/SiC + graphite(Gr) composites at very low speed (<2 m/s) and load (<300 N) conditions have also noted good wear resistance [2,5,6]. At higher sliding speeds and loads of more than 4 m/s and 100 N respectively, different wear mechanisms may be predominant due to complex interactions of thermal loading and deformation. Importantly, the localization of frictional heat on the sliding surface may cause thermally induced micro-cracking and a concomitant reduction in the wear resistance and fracture toughness [7]. To withstand the high interface temperatures, brake materials should possess high thermal stability and thermal conductivity to effectively dissipate the generated heat. Further, the crack resistance of the composites should be high to avoid catastrophic failure during emergency braking conditions. While the presence of ceramic particles improves the wear resistance, it proves detrimental to the overall thermal conductivity and crack resistance.

Traditionally, metal matrix composite brake pads comprise of a uniform distribution of ceramic particles in a metal matrix. Noting that the contrasting requirements of high wear resistance and thermal conductivity are separated spatially, Prabhu et al. [8] have studied the wear properties of layered Fe/SiC composites. In this approach, the layers of different physical, mechanical, and thermal properties are built into the composite to optimize the properties. These composites have been termed multi-layer composites (MLC) [9,10], and are a subclass of functional graded materials. MLCs possess a sharp change in microstructure and/or composition along a given direction. MLCs have been found to be promising candidates in many applications such as in dental implants, thermal barrier coating, cutting tools, solid oxide fuel cells, semiconductor devices, bullet-proof vests and armor plates [11]. Hunt et al. [12] and Erdogan [13] suggested that the presence of reinforced and unreinforced regions in the MLC reduced the driving force for crack propagation and thereby improve toughness. Arslana et al. [7] processed a three-layer alumina based composite by powder metallurgy and showed improved fracture

* Corresponding author. Tel.: +91 953 553 1407; fax: +91 80 2560 5362.
E-mail addresses: ramprabhu.t@gmail.com (T. Ram Prabhu), srikanth@iitm.ac.in (S. Vedantam).

http://dx.doi.org/10.1016/j.wear.2014.06.006
0043-1648/

toughness, damage resistance and thermal conductivity compared to conventional single layer composites. They also suggested that the layer structure may present potential in improving the wear resistance of the composites. The numerical model by Leon [14] showed that a discrete graded structure may improve damage resistance and toughness. We note that most of these studies on graded composites have been focused on the fracture mechanics aspects [13,15]. A study of the wear resistance by Prabhu et al. [8] of multilayer Fe/SiC composites showed that the layer structure provides promising wear and friction properties compared to uniform Fe/SiC composites. However, to our knowledge, there have been no studies of the tribological properties of multilayer Cu matrix hybrid composites at a range of sliding speeds (5–35 m/s) and high load (2000 N) conditions.

In this work, we have studied layered composites with particle size gradients as well as composition gradient by varying the size and volume fraction of the SiC particles. The layered composites have an outer layer consisting of a composite to provide strength, thermal stability, wear resistance and an inner metallic layer to improve bulk thermal conductivity, toughness and damage resistance. In addition, the composite layers were hybridized with a graphite solid lubricant to stabilize the friction at high temperature [16]. Also, the addition of graphite in the Cu/SiC composites improves thermal conductivity, machinability, damping and anti-seizure properties [5,6]. These layered composites were studied at a range of sliding speed conditions (5–35 m/s) to understand their dry sliding wear and friction behavior. In addition, the mechanical and microstructural characterization of the composites has been carried out. The potential wear mechanisms and elements/compounds present in the wear surface as well as the fracture surfaces were studied.

2. Experimental procedures

2.1. Materials processing

For the preparation of the composites, the raw material powders used were commercially pure powders of copper, tin, SiC, barium sulphate, graphite and zinc stearate. The mean size, purity, grade, apparent density and manufacturer of the powders are given in Table 1. We have processed two types of multilayer hybrid composites (MLCs) using powder metallurgy. In addition, single layer composites (SLCs) of two types were also prepared for the purpose of comparison. The sequence of the layering and the thickness of each layer in the composites are shown in Fig. 1. The composition of the composite layer is 20% SiC, 20% graphite, 1% tin, 10% $BaSO_4$ and 49% Cu (% are in volume percent). It is noted that the purpose of addition of tin is to facilitate the liquid phase sintering for better densification. The small sizes of SiC particles were prepared by fragmenting the as-received large size SiC particles for 12 h in the ball mill with a ball to charge ratio of 6:1. The speed of ball mill was chosen to be 30 rpm to avoid excessive heating. The balls were 6 mm (diameter) SH 52100 ball bearing steel. The SEM images of both as-received large and small size particles of SiC are given in Fig. 2. The composite mixes were prepared using the mixing procedure described in Fig. 3. The powders were stacked in the order described in Fig. 1 in a low carbon steel cup and compacted in a 250 ton hydraulic press. The compact was annular in shape with an area, inner, outer radius of curvature, and a height of 3078 mm^2, 102 mm, 152 mm, and 6–7.5 mm respectively. Zinc stearate was applied to the die wall and punch to provide lubrication during ejection of the compact. The green compacts were further consolidated by a pressure assisted sintering process. The process parameters of compaction, sintering cycle and repressing are given in Fig. 4. It is noted that these process parameters were selected after a number of trials.

2.2. Testing

The density of the composites was determined according to the Archimedes method. The fraction of porosity was determined from the ratio of difference between the calculated and the measured density to calculated density.

Hardness measurements on the composite surfaces were performed using a Brinell hardness tester (Wolpert Universal Hardness Tester) under the load of 10 kg. At least five measurements were taken and the average value is reported. A SEM was used to characterize the size of the SiC particles. We used *Image J* software to measure the sizes of the particles from the SEM images.

The wear and friction behavior of the composites were studied using a computer controlled pad-on-disk laboratory scale inertial brake dynamometer in air at ambient temperature (25–30 °C). The schematic of the dynamometer, the sample preparation and the burnishing procedure of the samples were given in our earlier paper [17]. Two samples from each composite were polished, cleaned in acetone before testing. The swept radius and area of the composites were 51.5 mm and 3078 mm^2 respectively. An AMTY 273-68 grade gray cast iron (C: 3–3.6%, Si: 1.6–2.3%) disc was used as a counter surface. The disc has a diameter and a hardness of 500 mm and 225 BHN respectively. The brake disc was thoroughly cleaned with proprietary brake cleaning agents to eliminate grease, surface residue or any debris between tests. The operation of the brake dynamometer and test procedure were described in detail elsewhere [18]. The brake testing parameters of the composites are given in Table 2. The main braking variables such as the stopping distance and friction coefficient (CoF) were recorded by a data acquisition system. The mass loss of the samples was determined using an Osaka Digital (XB 220A) electronic balance with a precision of ± 1 mg. The volume loss per unit sliding distance was taken to be the wear rate of the composites.

The microstructure analysis was performed in the composites using a stereoscope (SEIWA) and inverted optical microscope

Table 1
Characteristics of powders.

Powder	SiC	Graphite	$BaSO_4$	Sn	Cu
Mean size (μm)	195[a], 45[b]	125	75	50	75
Purity (%)	95	95	95	99	99
Density (g/cc)	3.2	2.2	0.658	4–4.2	2–2.4
Grade	α-SiC (6-H)	Natural (flaky)	IS 64-1992 Gr:2, Type I	Atomized	Electrolytic
Manufacturer	Grindwell Norton Ltd, Mumbai	Oxeeco Technologies Pvt Ltd, Hyderabad	Industrial Chemicals & Acids, Bangalore	M/s Kandoi Metal Powder Ltd, Jaipur	M/s Kandoi Metal Powder Ltd, Jaipur

[a] Large size ceramic particles.
[b] Small size ceramic particles.

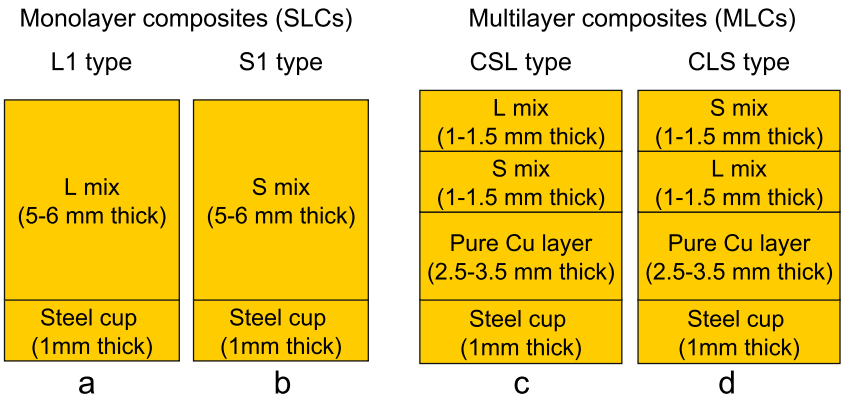

L mix: 49% Cu - 20% SiC (180-210 μm) - 20% Graphite - 10% $BaSO_4$ - 1% Sn (% in vol %)

S mix: 49% Cu - 20% SiC (30-60 μm) - 20% Graphite - 10% $BaSO_4$ - 1% Sn (% in vol %)

Pure Cu layer - 100% Cu (% in vol %)

Steel cup: Low carbon steel (C 20 grade, Fe-0.15-0.25% C)

Fig. 1. Stacking sequence of layers in the single and multi-layer Cu/SiC + Gr composites.

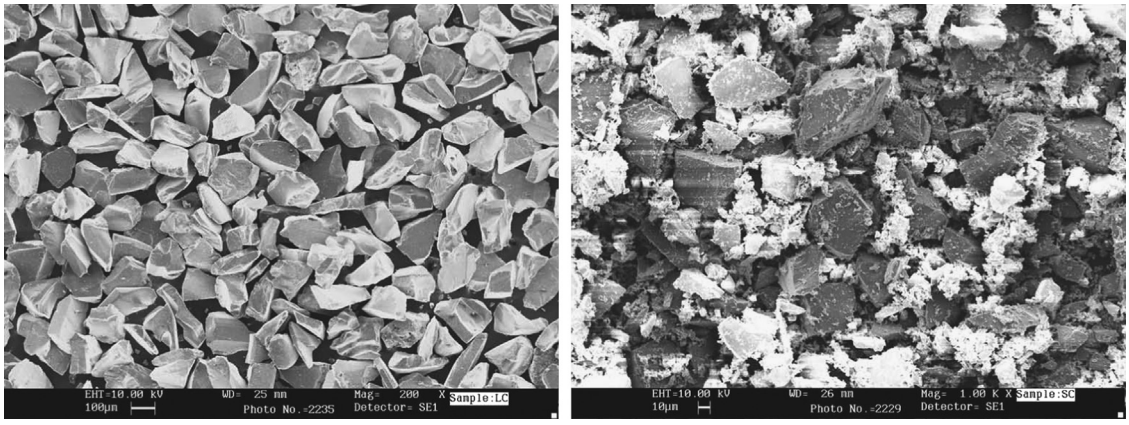

Fig. 2. SiC particles: (left) as received large size powders (180–210 μm) and (right) small size powders (30–60 μm).

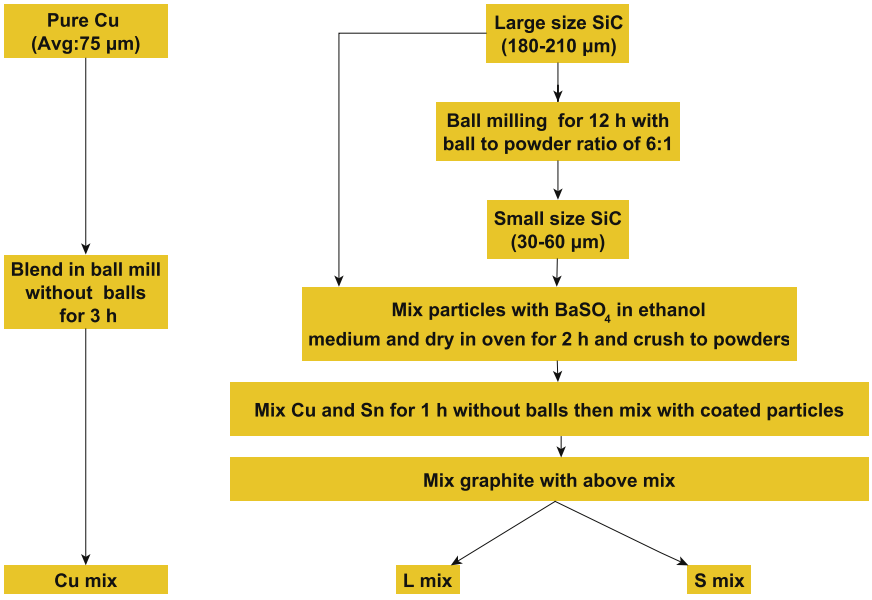

Fig. 3. Mixing procedure for preparation of copper and composite mixtures.

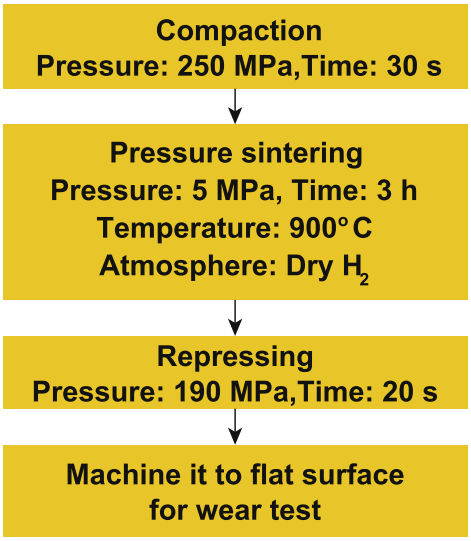

Fig. 4. Process parameters for preparation of composites.

Table 2
Brake testing parameters of dry sliding wear tests.

Rotor sliding speed (m/s)	Load (N)	Braking energy (kJ)	No. of braking stops	Moment of inertia of the flywheel (N ms^{-2})	Speed of rotor (rpm)
5	2000	8	30	40	191
10	2000	31	30	40	382
30	2000	282	30	40	1146
35	2000	385	30	40	1337

(Nikon Epiphot). The topography of the surface and sub-surface of worn samples were analyzed in a SEM (ZEISS/LEO 440i/FEI-SIRION) and stereoscope. A Shimadzu 6000 x-ray diffractometer fitted with a copper tube and graphite monochromator of Cu Kα radiation was used to analyze the worn surface of the composites. XRD patterns were recorded over a 2θ range of 10–90° using a step of 0.028° and at a rate of 0.68°/min.

Two samples from each group of composites were cut in a low speed diamond saw cutter and polished to the dimension of 10 mm × 10 mm × 8 mm for performing compression tests. The compression tests were carried out in a universal testing machine at a strain rate of 0.001 m/s. The average value of the compressive strength is reported.

The composites were tested for flexural strength according to the DIN 50110 standard. A three-point bend test set up was used to characterize the flexural properties of composites. The bending load was applied perpendicular to layer alignment on the steel cup so that the composite layers were under tension. The tests were performed in a TIRA 2820S universal testing machine at a cross head speed of 1.67×10^{-5} m/s. The sample dimensions and load span length were 60 mm × 15 ± 1 mm × 8 ± 0.5 mm and 50 mm respectively. The flexural strength of the composites was determined using the relation

$$\sigma_f = \frac{3Pl}{2Bt^2} \quad (1)$$

where P is the maximum load at fracture, l the span length, B the width of and t the thickness of the sample. The fracture surfaces were then characterized using SEM and stereoscope to identify the microscopic failure mechanisms.

Table 3
Density and % porosity of the composites.

Types	Designation	Theoretical density (g/cc)	Measured density (g/cc)[a]	Fraction of porosity (%)
Single layer composites (SLCs)	L1	6.22	5.73	7.9
	S1	6.22	5.76	7.4
Multi layer composites (MLCs)	CLS	7.02	6.83	2.7
	CSL	7.02	6.82	2.9

[a] Standard deviation for the measured density values = 0.022.

3. Results and discussion

3.1. Density and porosity

The density and % porosity of the composites are shown in Table 3. The MLCs possess higher density than the SLCs due to the presence of high density Cu layer in the MLCs. However, it is interesting to see that the Cu layer in the MLC has a low porosity as seen in Fig. 5 primarily due to the higher diffusivity of Cu atoms. The higher density of MLCs shows that the sintering cycle chosen is appropriate for the fabrication of MLCs.

3.2. Characterization of layer interface

The layer structure of the representative MLC (CLS composite) and SLC (L1 composite) samples is shown in Figs. 5 and 6. The SEM image and micrograph distinctly show size gradient of the SiC particles along the top two hybrid composite layers and the SiC volume fraction gradient along the second and third layers. There is no evidence of diffusion of SiC or of graphite particles between the composite layers or between the composite layers and Cu layer. The interlayer of the composite is continuous, uniform and free of debonded regions, clusters of particles or defects. Further, the distributions of the SiC (grey color) and the graphite (black color) in the composite layer are uniform without any clustering in both the MLCs and SLCs, as seen in Fig. 5(b–d). Macrographs in Fig. 6 also show the continuity of layers clearly in the MLCs and SLCs. The bonding of interface of the composite and the Cu layer is of good quality because of the Cu present in both the layers. The sound bonding between the steel and the Cu layers (as seen in Fig. 5(a)), the Cu layer and the composite layer (as seen in Fig. 5(c)), and the composite layers (as seen in Fig. 5(b)) confirm that the selected process parameters are appropriate to process sound quality layer structure in the Cu matrix hybrid composites.

3.3. Wear behavior

3.3.1. Wear rate

The wear rates (volumetric loss per unit sliding distance) of the composites are shown in Fig. 7. The MLCs (CLS and CSL) show lower wear rate at all sliding speeds (5, 10, 30 and 35 m/s) compared to SLCs (L1 and S1). This behavior is more pronounced particularly at 5 and 10 m/s. The wear rate of the composites reduces with sliding speeds. The interface temperature increases sharply with increasing sliding speeds due to the conversion of higher kinetic energy to thermal energy during braking. This causes oxidation of the contact couple and the rapid removal and regeneration of the tribolayer at the interface. Consequently, the friction at the interface decreases (as discussed later) so significantly that the rate of increase of stopping distance over the rate of mass loss increases as a consequence. Thus, the wear

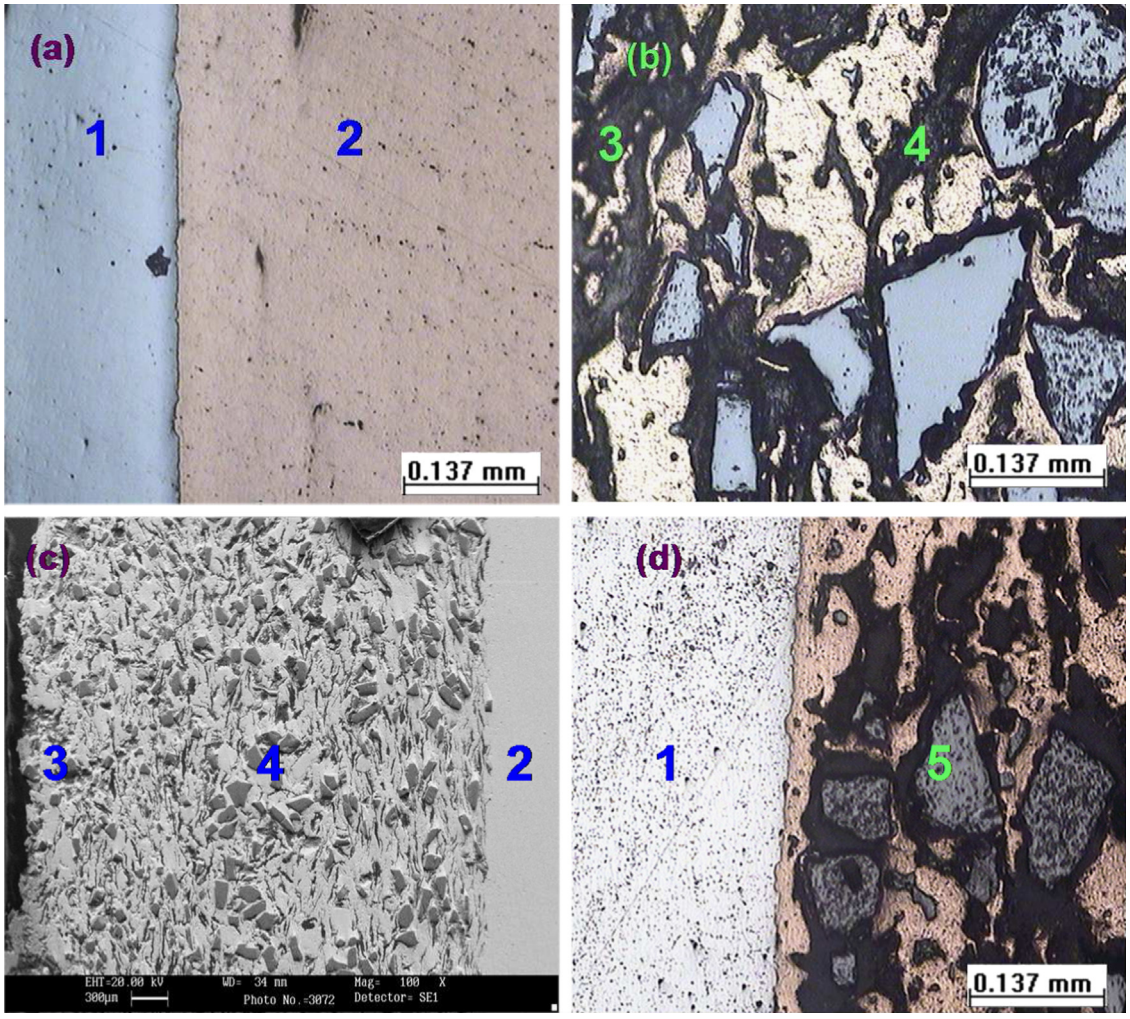

Fig. 5. Microstructure of the Cu/SiC + Gr composites, (a) and (b) show the layer transition from back cup to Cu layer, and the small size SiC to the large size SiC composite layer in a CSL type multilayer composite, (c) SEM image shows the SiC particle size gradient in a CLS type multilayer composite, (d) L1 type single layer composite. (1) Back cup, (2) Cu layer, (3) composite layer of small size SiC particles, and (4) and (5) composite layer of large size SiC particles.

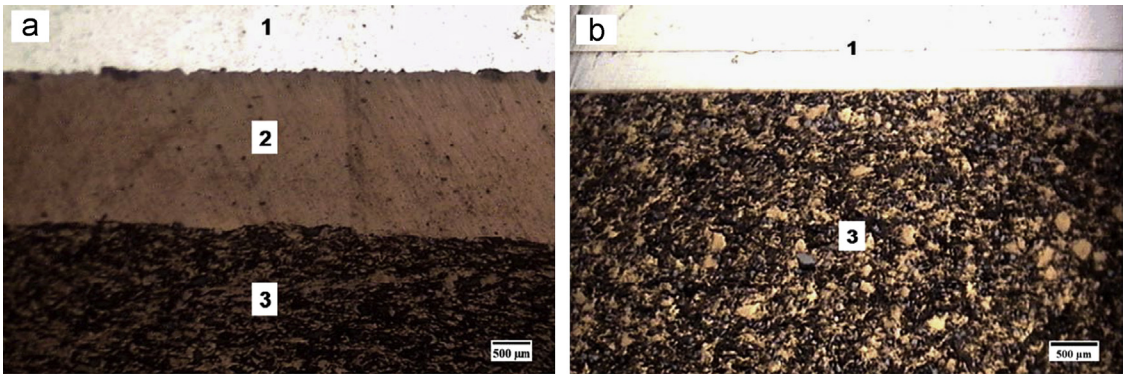

Fig. 6. Layer structure of the Cu/SiC + Gr composites, (a) CLS type multilayer composite, (b) L1 type single layer composite. (1) Back cup, (2) pure Cu layer, and (3) composite layer.

rate reduces with sliding speed up to a critical speed of 30 m/s. Beyond this speed, the wear rate once again increases due to increased effects of oxidation, matrix softening and cracking, and delamination wear, as observed in Fig. 7. This behavior of decreasing wear rate with increasing sliding speed has also been observed in the Al 7091/20%SiC alloy by Wank et al. [19]. However, it is to be noted that the mass loss of the composites increases with sliding speed. Unlike the wear rate (volumetric loss per unit sliding distance) which also depends on the stopping distance and density, the mass loss is a single measurable value indicating the amount of material removed. The increase of interface temperature with increasing sliding speed/braking energy significantly enhances the mass loss by oxidation, the matrix softening and cracking and delamination wear.

At sliding speeds of 5 and 10 m/s, the graphite embedded in the matrix remains in the bulk, as is evident from Fig. 8(a and c). Further, the absence of oxidized scales in the macrographs of the composites indicates that the interface temperature is not high

enough to cause oxidation of the composites. By comparing the braking energies dissipated between 5–10 m/s and 30–35 m/s sliding speeds as given in Table 2, we see that the amount of heat generated at 5–10 m/s much lower than that at 30–35 m/s. The deformation behavior of the surface and subsurface of the composites and area fraction of the particles at the surface affect the wear rate of the composites. The formation of a fine grain matrix is stimulated by reducing the particle size in the composite and providing more nucleating sites for grain formation during sintering [20]. In addition, the effects of plastic strain gradient, geometrically necessary dislocation density in the matrix, particle pinning increase for small size particle reinforcements [21]. As a consequence the composites with small size SiC reinforced composites at the sliding surface layer (S1 and CLS) have higher strength and this minimizes the wear loss significantly at 5 m/s. The greater area fraction (smaller inter particle spacing) of the small size SiC particles minimizes matrix wear by preventing the metal (Cu matrix) to metal (cast iron countersurface) adhesive contact and ploughing of the matrix by the hard abrasive wear debris.

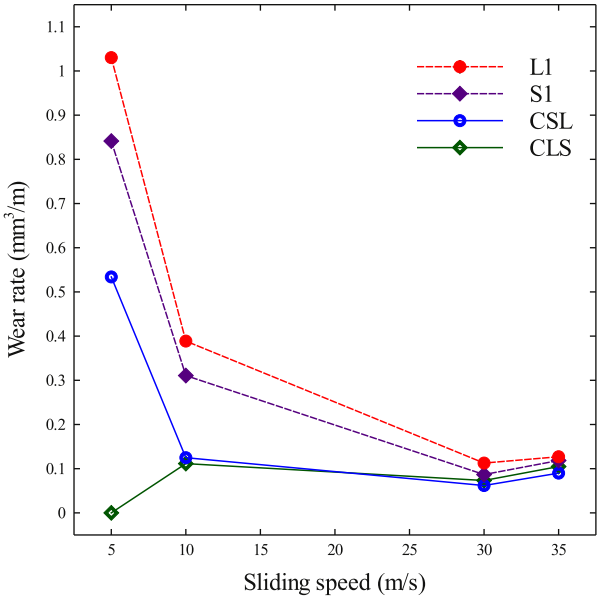

Fig. 7. Wear rate of the Cu/SiC + Gr composites.

At sliding speeds above 5 m/s, the size effects become less pronounced. Compared to SLCs (L1 and S1) the MLCs (CLS and CSL types) show lower wear rates for which the explanation has been discussed earlier. With increasing sliding speeds, the interface temperature increases, resulting in the formation of oxides on the sliding surface, decrease of the flow stress of the matrix and weakens the bond between the Cu matrix and SiC particles facilitating easy pull out [22]. At 30–35 m/s, the difference in the wear rate of the composites is not significant compared to 5 m/s. This is mainly due to the formation of a mechanical mixed tribolayer (MMTL) at the composite surface. The fragmented wear debris gets milled and mixed at 30–35 m/s. The debris consists mainly of oxide scale, fractured pull out particles, material transferred from the counter surface and sheared graphite. The debris spreads uniformly over the surface and forms the MMTL. MMTL formation is accelerated with sliding speed leading to the better coverage at 30 m/s. However, beyond certain sliding speed (30 m/s), the critical thickness of the tribolayer is reached quickly and breaks up quickly leading to increased wear rate. The tribolayer prevents the three body abrasive wear and adhesive

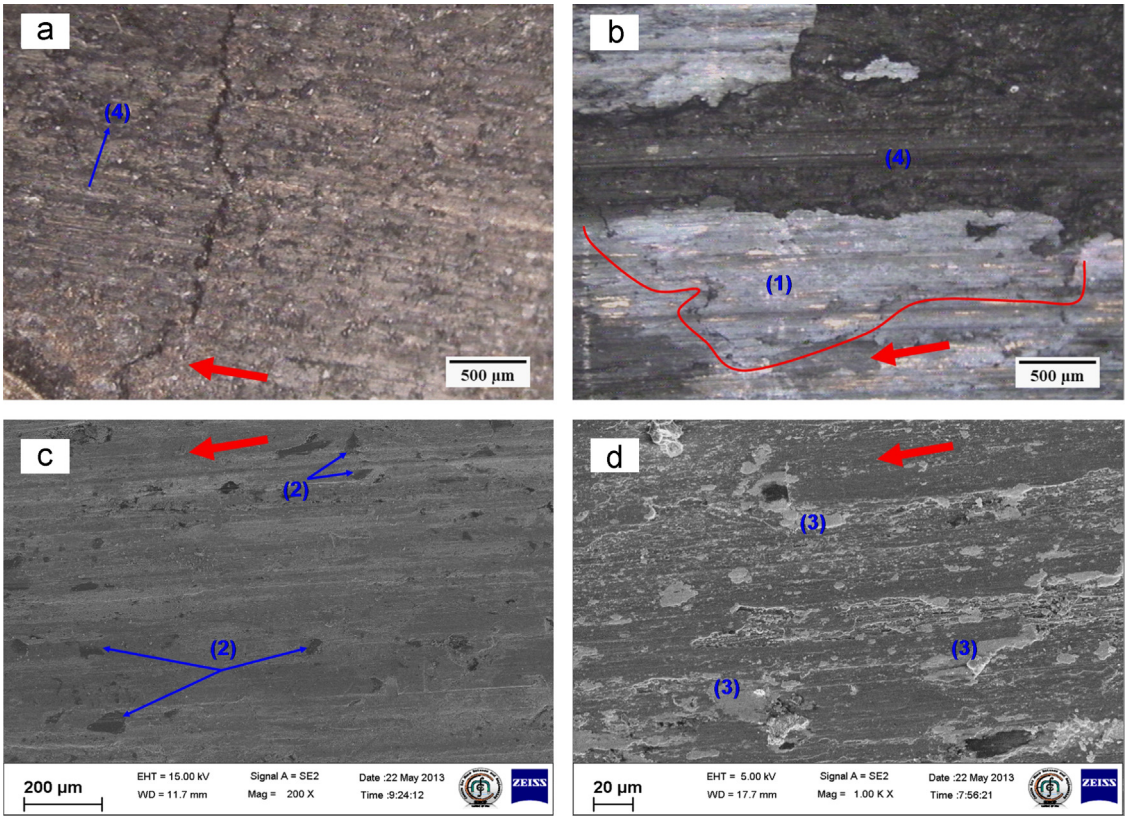

Fig. 8. Wear surface morphology of the CLS type multilayer composite, (a) and (b) macrographs and (c) and (d) SEM images of composite tested at 10 m/s and 30 m/s respectively. (1) Oxide scale, (2) particles protruded on the surface, (3) tribolayer, and (4) groove lines. Arrow shows the direction of sliding. The curve line shows the wear sheet removed by delamination.

contact between contact surfaces [23]. Compared to the SLCs (L1 and S1), the MLCs (CLS and CSL types) only show a slightly higher wear resistance.

3.3.2. Wear mechanisms

The macrographs and SEM images of the surface of a representative wear tested MLC (CLS) are shown in Fig. 8. Grooves are mainly observed in the samples tested at 5 and 10 m/s. No oxide scales or deformed graphite layers are seen on the surface. There is no trace of a tribolayer on the composite surface. This is also verified by XRD analysis. A XRD pattern of the same composite tested at 10 m/s, as given in Fig. 9(a), shows strong peaks of Cu and SiC. These strong peaks suggest that the temperature at the interface is not sufficient to cause oxidation. The absence of large wear patches or pits and thick oxide scale also support this observation. Venkataraman et al. [24] suggested that sub-surface turbulent plastic flow, in addition to hard reinforcing particles, may also be important for the formation of the tribolayer. The subsurface of the composites tested at 10 m/s, as shown in Fig. 10(a), is not severely enough deformed to exhibit the plastic flow. Hence, the tribolayer is not formed in these composites at 5–10 m/s. Thus we conclude that abrasive wear is the dominant mechanism at 5–10 m/s. The observation of an intermetallic compound, Cu_6Sn_5, in the XRD pattern is probably due to a reaction between Cu and Sn during sintering. Surface cracks running normal to sliding direction are also observed in Fig. 8(a and c). These cracks originate mainly from the interfaces of the matrix and particles due to the differential thermal expansion of SiC and Cu during sintering. These cracks grow normal to sliding direction by tensile failure of surface layer [25]. Particularly, intergranular cracking around the particles and subsequent crack merging process allow wear sheets to be worn away by random, periodic mechanical and thermal loading. The abrasive action of counter surface asperities and loose wear debris exposes the SiC particles on the composite surface, as observed in Figs. 8(c) and 10 (a) of the composite tested at 10 m/s. Some of the exposed particles dislodge from the surface causing the third body wear. The third body wear particles plough the surface and form deep grooves. The participation of these protruding SiC particles and

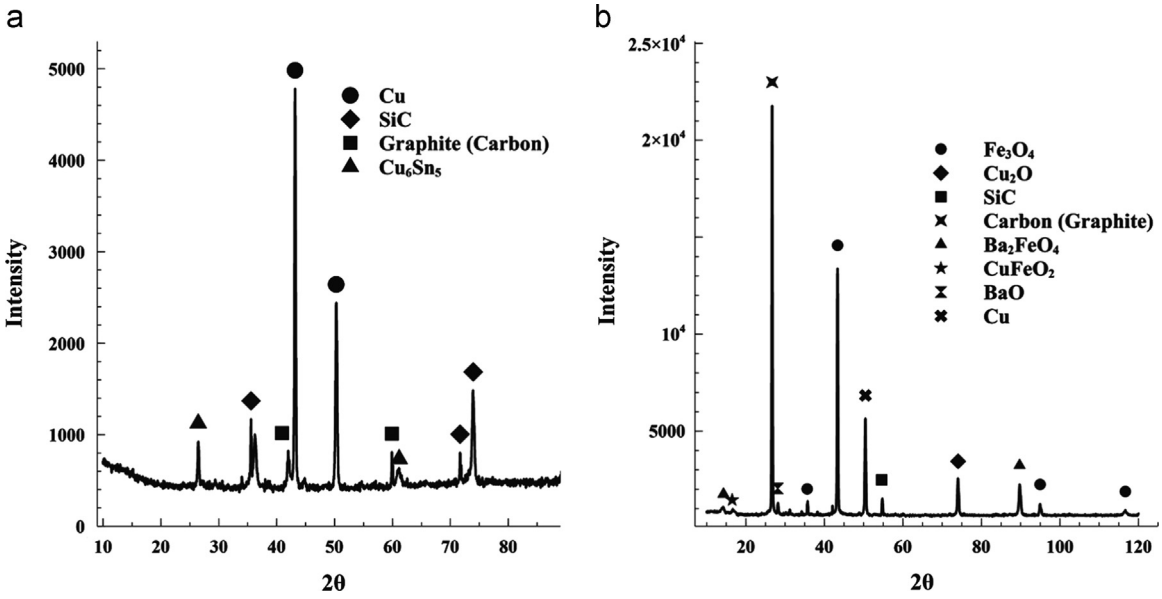

Fig. 9. XRD spectrums of a CLS type composite tested at (a) 10 m/s and (b) 30 m/s.

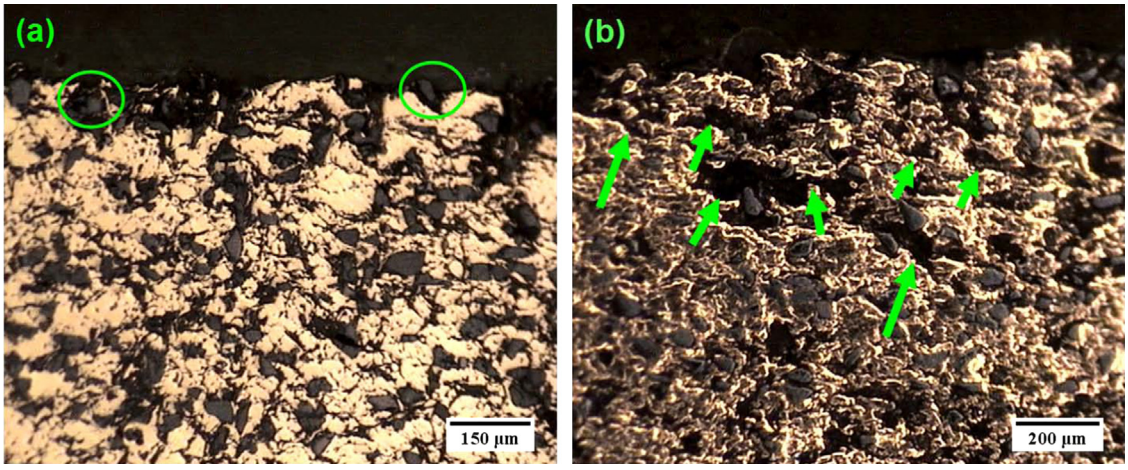

Fig. 10. Sectional view of the CLS type composite wear tested at (a) 10 m/s and (b) 30 m/s. Circle indicates the protruded SiC particles on the surface. Arrow indicates the delamination crack in the subsurface connecting particle interfaces.

third body wear debris in the friction processes enhances the friction coefficient and increases the wear rate sharply at 5–10 m/s. In summary, abrasive wear is a main mechanism at sliding speeds of 5–10 m/s.

At 30 and 35 m/s, thermal effects are clearly noted by the presence of oxide scales. A representative XRD pattern of the sample tested at 30 m/s is shown in Fig. 9(b) and mainly shows a mixture of simple and complex oxides of the composite and countersurface constituents. The thickness of the oxide scales increases with sliding speeds. The presence of Fe_3O_4, Ba_2FeO_4 and $CuFeO_2$ on the wear surface confirms a significant interdiffusion of Fe atoms from counter surface into the composite during sliding. The metallic oxides, especially iron oxides, play a vital role in stabilizing the tribolayer by pinning dislocations and acting as a solid lubricant [23,26,27]. The high intensity peak of graphite shows that the composite surface is also extensively covered with graphite. The high magnification image of the wear surface, as given in Fig. 8(d) shows a uniform, light gray color tribolayer on the composite surface. The tribolayer reduces and stabilizes the friction coefficient and wear rates at 30–35 m/s. The above observations show that the temperature and deformation effects are dominant at sliding speeds of 30–35 m/s, and that tribo-oxidation and the formation of a tribolayer play a vital role in determining the wear and friction behavior of the composite. Further, the high temperature at the interface softens the matrix and weakens the interfaces of the matrix/particles of the composite. Early removal of wear debris from the surface leaves the surface uneven and irregular. Consequently, uneven contact load distribution makes the periodic loading concentrated on discrete regions of the contact surface. Cracks initiate and grow by the fatigue frictional loading from the alternate cooling and heating of the surface of the samples resulting higher mass loss at sliding speeds of 30 and 35 m/s. At the same time, the minimization of friction by tribolayer enhances the stopping distance and maintains the wear rate at sliding speeds of 30 and 35 m/s. The cyclic loading occurs because of thermoelastic and thermoplastic instabilities in sliding at high sliding speeds [25]. The observation of craters is indicative of extensive deformation of the sub-surface region which releases the sheets of material from the surface during wear. Fig. 10(b) shows the subsurface of the composite tested at 30 m/s. A heavily work hardened zone and delamination cracks are observed at the subsurface. The repeated sliding at high contact load accumulates strain at the subsurface. The accumulated strains help microcracks nucleate at the voids in the subsurface. These propagate parallel to the sliding direction towards the wear surface by connecting interface sites of particles and matrix, Fig. 10(b), leading to delamination of material from the surface. In summary, a mixed mode of wear mechanisms such as tribooxidation, delamination, abrasion and thermal fatigue wear are observed at 30 and 35 m/s.

3.4. Braking behavior

The variation of the mean friction coefficient and mean stopping distance with sliding speeds for the composites are shown in Figs. 11 and 12. The friction coefficient reduces with sliding speed for all composites. Uyyuru et al. [28] also observed a similar behavior of decreasing friction coefficient and wear rate with increasing sliding speeds in Al matrix composite/brakepad tribo-couple. The friction at the interface is affected by many variables such as the surface microstructure, bulk toughness, thermal conductivity, countersurface material properties, surface roughness and wear debris trapped at the interface among others. The formation of an oxide scale, greater participation of graphite in the sliding, diminishing adhesive and abrasive frictional contacts reduce the frictional forces at the interface with increasing sliding speeds.

The effect of particle size on the friction coefficient is observed especially at 5 m/s. The large particle sizes appear to be better in giving higher friction than the small particle sizes. However, this

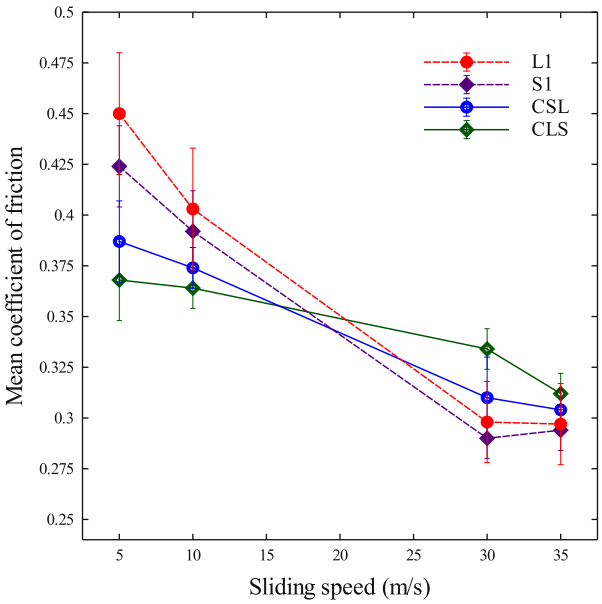

Fig. 11. Effect of sliding speed on mean friction coefficient of the composites (load: 2000 N, No. of stops: 30).

high friction is the effect of third body wear. Early removed wear debris with large size abrasive particles provides high friction. For example, the L1 composites show a very high friction coefficient of 0.455 at 5 m/s. This high friction does not translate into improving braking performance or wear resistance, as can be seen from the higher stopping distance (as in Fig. 12 (a)) and wear rate (as seen in Fig. 7) of L1 composite at 5 m/s.

Above 5 m/s, the variation in the friction coefficient of the SLCs or MLCs is within the error bar. Hence, the effects of particle size in the SLCs or layer sequence in the MLCs are negligible. The formation of tribolayer helps in stabilizing the friction above 5 m/s.

Between SLCs (L1 and S1) and MLCs (CLS and CSL), MLCs appears to provide high consistent friction with less variability with increasing sliding speeds. The advantage of the layer structure of the MLCs is clearly seen at 30–35 m/s wherein a controlled high friction coefficient with less variability is achieved for multilayer composites (CLS type). The higher thermal conductivity of the layered composite reduces the rates of oxidation and matrix softening rate. Similarly the improved toughness of the layer structure improves the frictional load distribution and minimizes the stress localization at the surface. These factors help in providing relatively higher controlled friction in the MLCs.

The stopping distance is an important braking performance parameter and is a strong function of the friction coefficient. As seen in Fig. 12(a), the variation of stopping distance is quite negligible in both the SLCs and the MLCs at 5–10 m/s in contrast to the high variation observed at 30–35 m/s (as seen in Fig. 12(b)). This variation is mainly due to the complex interaction of different wear mechanisms. Since the stopping distance depends on the friction coefficient, the influence of the particle size and layer structure on the friction coefficient is also applicable to the stopping distance.

3.5. Mechanical behavior

3.5.1. Compression strength

The compression strength of the MLCs is higher than SLCs, as given in Table 4. As explained by Lin et al. [29] during compression, the metal matrix composites deform mainly by two mechanisms, namely matrix grain deformation and boundary slip deformation. The boundary slip deformation mode increases with increasing volume fraction of particles. Compared to the SLCs, the

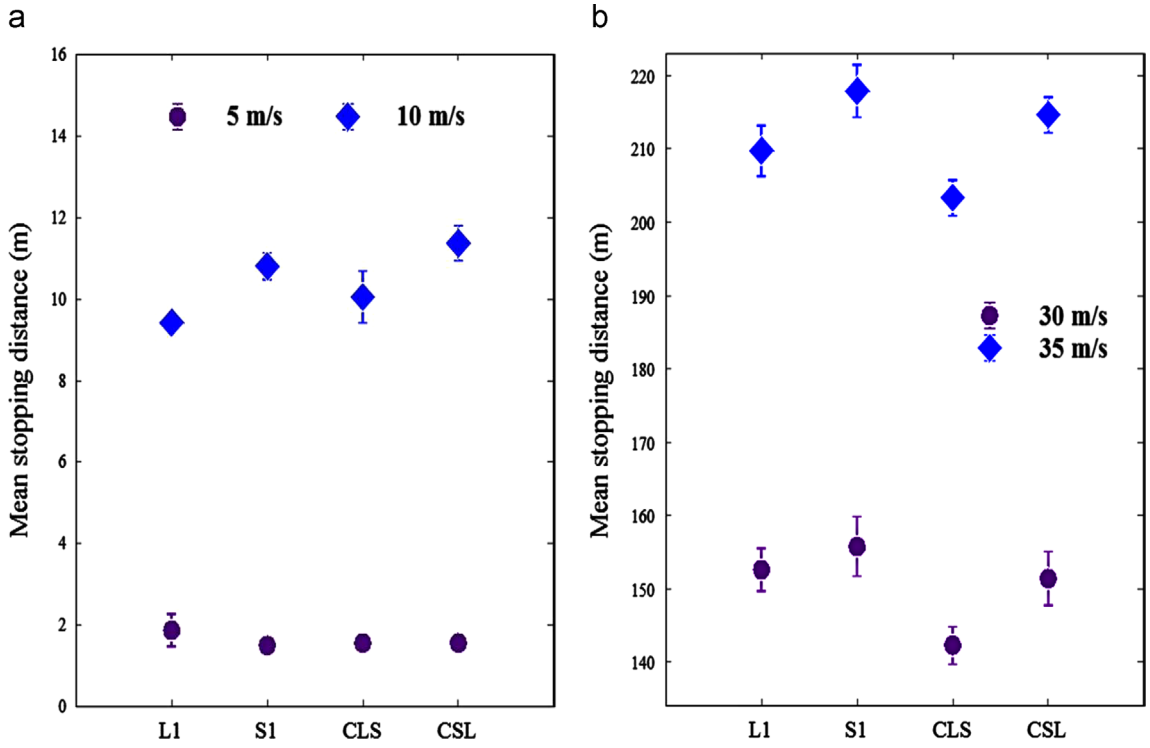

Fig. 12. Effect of sliding speed on mean stopping distance of the composites (load: 2000 N, No. of stops: 30).

Table 4
Mechanical properties of Cu/SiC + Gr composites.

Types	Designation	Compression strength (MPa)	Flexural strength (MPa)	Surface hardness (BHN)
Single layer composites (SLCs)	L1	159 ± 9	46	67 ± 4
	S1	153 ± 3	56	70 ± 3
Multi layer composites (MLCs)	CLS	196 ± 8	95	71 ± 2
	CSL	207 ± 5	96	69 ± 3

MLCs undergo lower boundary slip deformation due to lower overall volume fraction of particles resulting in a higher compression strength. In addition, the relatively lower porosity and strain hardening of the Cu layer contribute to the higher compression strength of MLCs. During compression, the Cu layer begins strain hardening after the failure of a composite layer. The strain hardened Cu layer during compression is shown in Fig. 13. The effect of the sequence of layer arrangement on the compression strength is negligible in MLCs. The particle size effect on the compressive strength of single layer composites is also not significant. The large size particles impede the plastic flow of matrix more effectively than the small size particles during compression [29]. The variation of the surface hardness amongst the various composites is also quite negligible.

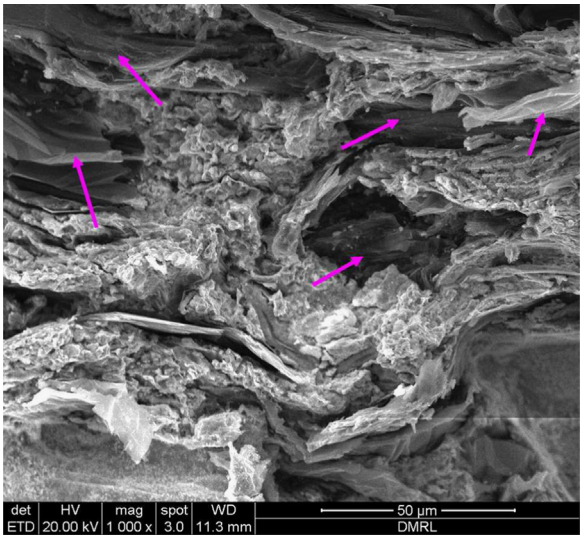

Fig. 13. Strain hardened Cu layer in the CLS composite tested in compression. Arrows indicate the severely plastic deformed Cu sheets flowing normal to the compression loading direction. Also, the slip lines are observed inside the Cu sheets.

3.5.2. *Flexural strength*

The flexural strengths and the force vs. deflection curves of the composites are given in Table 4 and Fig. 14 respectively. The flexural strength also follows the same trend as the compressive strength of the composites. Porosity significantly affects the flexural strength of the composites. The low porosity in the MLCs (CSL and CLS) gives them their higher flexural strength. In addition, the presence of residual compressive stresses in the composites contribute to the strengthening of MLCs. These residual stresses arise from different thermal expansion behaviors of the metallic and composite layers [30]. The layers with lower or higher thermal expansion develop compressive or tensile stresses respectively. Using a deformation model of the functionally discrete graded Al/SiC composites, Leon [14] predicted that the region of low particle density determines the stiffness and failure strain of the composite. In the present case, this would be the Cu layer which is the particle free. The low stiffness and high failure strain of the Cu layer gives multilayer composites lower stiffness and higher failure strain compared to single layer composites. In addition, the presence of tensile residual stresses in the Cu

matrix contributes to the earlier yielding of the MLCs [21]. Arslana et al. [7] also observed that the bending strength of three-layer alumina based composites is much greater than that of single layer alumina composites. They attributed the better flexural properties

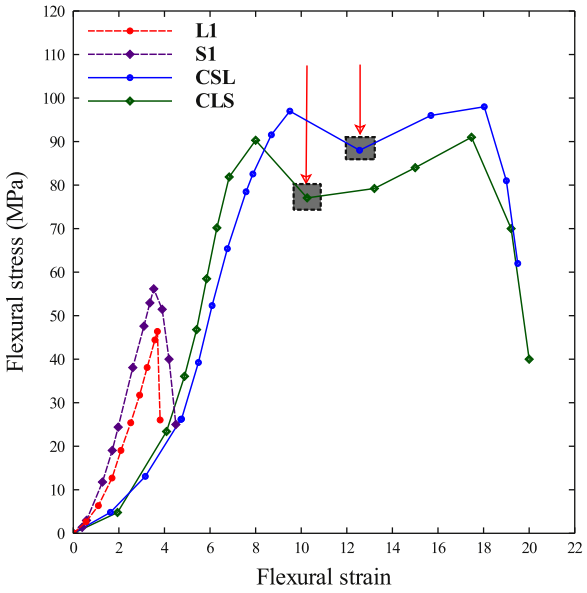

Fig. 14. Flexural test curves of the composites. Shaded regions indicate a drop and rise in the curve. The drop and rise represent the failure of the composite layer and the onset of the work hardening of the Cu layer respectively in the multilayer composites.

to residual compressive stresses in the outer layer. The soft Cu layer blunts and deflects the crack running from composite layers.

The observations of local minima (shaded regions in Fig. 14) in the force–deflection curve of the MLCs indicate the onset of the plastic deformation of Cu layer. The subsequent rise in the load is due to the work hardening of the Cu layer. Zechnera et al. [31] have observed similar trends in the force–displacement curves of aluminium multilayer composites and showed that the introduction of soft polymer layer in the Al multilayer composite significantly improved its crack growth resistance.

The effect of layering sequence on flexural strength is negligible in the MLCs. This result is in accord with the Leon model [14] which shows that the different arrangements of particle size gradient in multilayer composites do not have any influence on strength and failure strain.

In the single layer composites, the small size particles in the matrix (S1) have smaller interparticle spacing between particles in the composite. The reduction in the spacing provides greater geometric constraints to easily deforming Cu matrix during deformation and enhances the dislocation–particle interaction [32]. In addition, the small size particles have a larger total interfacial area. The analytical model developed by Arsenault et al. [33] showed that the thermally induced dislocation density around the interface is directly proportional to the particle surface area. These dislocations are formed to relax the thermal strain developed by the differential thermal contraction effect of particles and the Cu matrix. The substructure formed by the forest of dislocations makes deformation more difficult by dislocation density strengthening. The chance of particle fracture reduces with smaller particle size because of less probability for existence

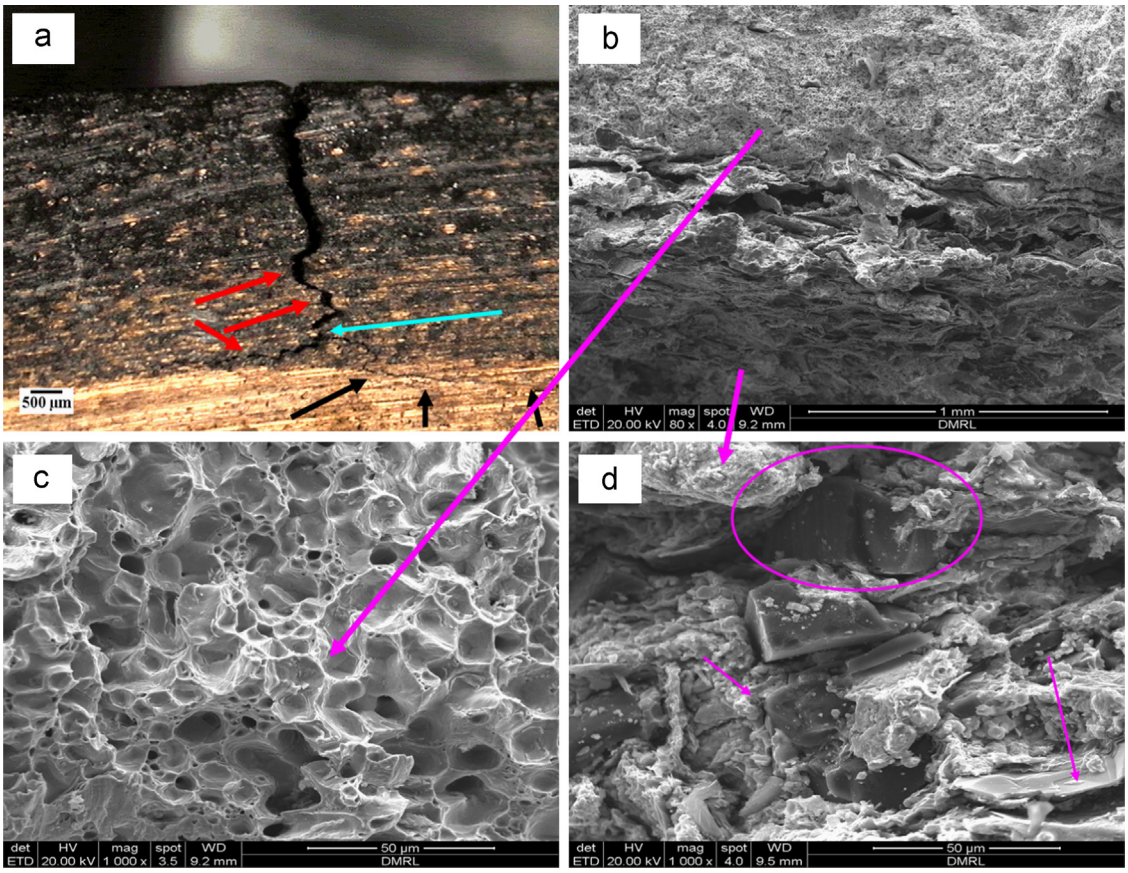

Fig. 15. Fractographs of the flexural tested CLS composite. (a) Macro-view of the cross section shows crack arresting and branching at the Cu/composite layer, crack tip blunting in the Cu layer, (b) sectional view of the fracture surface, (c) pure ductile failure of Cu layer showing elliptical dimples, and (d) quasi-cleavage intergranular fracture of the composite layer showing cleavage facets and cracks around the particles with no evidence of particle cracking.

of defects [21]. In summary, the geometric constraint, limited particle fracture and high dislocation density enhance the flexural strength of the S1 composites.

3.5.3. Fractography

A cross sectional view of the flexurally tested CLS composite is shown in Fig. 15(a). The application of the bending load makes the top composite layer experience tensile stresses. When the load on the composite layer reaches a maximum, debonding of the Cu/SiC interface begins at the voids. A crack develops from the voids and soft graphite particles and propagates in the matrix, and connects other sites of Cu/SiC and Cu/Gr interfaces. The crack path in the top composite layers shows the turtle path connecting all interface sites. From this, we understand that the particle/matrix interface plays a key role in the fracture behavior of the composite layer. While the crack approaches the interlayer of composite and pure Cu layer, the soft Cu layer blunts the crack tip and deflects the crack from the composite layers by reducing the stress triaxility, and increasing the plastic zone size around the crack tip. The enlargement of the plastic zone around the crack delays the propagation at the interlayer. This eventually delays the failure of the multilayer composites. Fig. 15(a) shows crack branching at the Cu/composite interlayer and a crack deflection by 30°–45° to the maximum tensile stress direction in the Cu layer indicating shear or ductile type of failure. The crack branching and crack tip blunting in the Cu layer in the MLCs ensures the failure of the composite layer completely before the failure of the soft Cu layer. This is useful to avoid catastrophic failure in service conditions. The flexural test samples show no evidence of complete debonding of composite and Cu layer indicating a sound bonding between layers in the composites.

The fracture surface of the flexural tested CLS composite examined under the SEM is shown in Fig. 15(b–d). The composite layer shows damaged particle/matrix interfaces suggesting that the shear stress at the interface has not exceeded the particle fracture strength. The particles restrict the motion of dislocations and reduce the plastic deformation. Shiny granular interfaces along with dull luster matrix in the composite layer indicate a quasi-intergranular cleavage fracture of the composite layer. The path of the crack around the particles, debonded particles, cleavage facets and dimples are observed in Fig. 15(b–d). There is no evidence of fractured particles in the composite layers. The fracture surface of the Cu layer shows elliptical dimples, characteristic of ductile failure, distributed through the entire layer as well as ductile tear ridges and porosity.

4. Conclusions

We have studied wear behavior of Cu/SiC + Gr hybrid composites in three multi-layer and two single layer configurations. The tribological and mechanical behavior of the composites were also evaluated and compared. The important findings are the following:

- The wear resistance and braking performance of the composites are increased by the presence of a layer structure in the composite. Small size particles are better in providing better braking behavior and low wear rate. A layered structure is more effective in providing better braking, especially at sliding speeds of 30 and 35 m/s.
- Abrasive wear is the main operative mechanism at 5–10 m/s whereas a mixed mode wear mechanism including oxidation, delamination, thermal-fatigue wear, abrasive wear is operative at 30–35 m/s.
- The compression and flexural strengths of MLCs (CLS and CSL) are significantly higher than SLCs. Lower porosity, strain hardening of the Cu layer and the residual compressive stress in the composite layer contribute to the higher strength. The effects of the layering sequence in MLCs and the particle size in SLCs on these properties are not significant.
- Crack growth resistance of multilayer composites is higher than the single layer composites due to the presence of the ductile Cu layer which deflects and blunts the crack. The fracture surface of the composite and Cu layers shows the quasi-cleavage intergranular fracture and the pure ductile fracture, respectively, in the multilayer composite.

Acknowledgments

We greatly acknowledge the materials and testing support rendered by HAL, Bangalore.

References

[1] G.C. Efe, M. Ipek, S. Zeytin, C. Bindal, An investigation of the effect of SiC particle size on Cu-SiC composites, Compos.: Part B 43 (2012) 1813–1822.
[2] Y. Zhan, G. Zhang, Y. Zhuang, Wear transitions in particulate reinforced copper matrix composites, Mater. Trans. 45 (7) (2004) 2332–2338.
[3] Th. Schubert, B. Trindade, T. Weibgarber, B. Kieback, Interfacial design of Cu-based composites prepared by powder metallurgy for heat sink applications, Mater. Sci. Eng. A 475 (2008) 39–44.
[4] S.C. Tjong, K.C. Lau, Tribological behaviour of SiC particle-reinforced copper matrix composites, Mater. Lett. 43 (2000) 274–280.
[5] C.S. Ramesh, R.N. Ahmed, M.A. Mujeebub, M.Z. Abdullah, Development and performance analysis of novel cast copper–SiC–Gr hybrid composites, Mater. Des. 30 (2009) 1957–1965.
[6] Y. Qin, Y. Wu, D. Wang, P. Li, X. Huang, Y. Zheng, Influence of SiC particle size on the wear properties of SiC/Cu composites, Adv. Mater. Res. 311–313 (2011) 635–639.
[7] G. Arslana, R. Janssen, N. Claussen, Processing and characterisation of three-layer alumina-based composites with enhanced damage tolerance, J. Eur. Ceram. Soc. 25 (2005) 3553–3561.
[8] T.R. Prabhu, V.K. Varma, S. Vedantam, High speed tribological and mechanical properties of layered Fe/SiC composites, J. Mater. Eng. Perform., April 2014, in press.
[9] K. Varuan, Functionally graded aluminum–matrix composites, Am. Ceram. Soc. Bull. 82 (2) (2003) 60–64.
[10] M.L. Pines, H. Bruck, Pressureless sintering of particle reinforced metal–ceramic composites for functionally graded materials: part I. Porosity reduction models, Acta Mater. 54 (2006) 1457–1465.
[11] S. Suresh, Graded materials for resistance to contact deformation and damage, Science 292 (2001) 2447.
[12] W.H. Hunt Jr., T.M. Osmand, J.J. Lewandowski, Structure–property relations in discontinuously reinforced aluminum (DRA) alloys, JOM 45 (1993) 30–35.
[13] F. Erdogan, Fracture mechanics of functionally graded materials, Compos. Eng. 5 (7) (1995) 753–770.
[14] L.M. Leon Jr., Functionally gradient metal matrix composites: numerical analysis of the microstructure–strength relationships, Compos. Sci. Technol. 66 (2006) 1873–1887.
[15] R.R. Castro, R.C. Wetherhold, M.H. Kelestemur, Microstructure and mechanical behavior of functionally graded Al A359/SiCp composite, Mater. Sci. Eng. A 323 (2002) 445–456.
[16] Y. Zhan, G. Zhang, The role of graphite particles in the high-temperature wear of copper hybrid composites against steel, Mater. Des. 27 (2006) 79–84.
[17] T.R. Prabhu, V.K. Varma, S. Vedantam, Effect of reinforcement type, size, and volume fraction on the tribological behavior of Fe matrix composites at high sliding speed conditions, Wear 309 (1 and 2) (2014) 247–255.
[18] T.R. Prabhu, V.K. Varma, S. Vedantam, Effect of SiC volume fraction and size on dry sliding wear of Fe/SiC/Graphite hybrid composites for high sliding speed applications, Wear 309 (1 and 2) (2014) 1–10.
[19] A. Wang, H.J. Rack, Transition wear behavior of SiC-particulate and SiC-whisker-reinforced 7091 Al metal matrix composites, Mater. Sci. Eng. A 147 (1991) 211–224.
[20] M. Barmouz, P. Asadi, M.K.B. Givi, M. Taherishargh, Investigation of mechanical properties of Cu/SiC composite fabricated by FSP: effect of SiC particles size and volume fraction, Mater. Sci. Eng. A 528 (2011) 1740–1749.
[21] N. Chawla, Y.L. Shen, Mechanical behavior of particle reinforced metal matrix composites, Adv. Eng. Mater. 3 (6) (2001) 357–370.
[22] M. Nosonovsky, P.K. Rohatgi, Biomimetics in Materials Science: Self-healing, Self-lubricating, and Self-cleaning Materials, Springer Series in Materials Science, vol. 152, Springer Science + Business Media, LLC, New York, 2012, http://dx.doi.org/10.1007/978-1-4614-0926-7.
[23] R.L. Deuis, C. Subramanian, J.M. Yellup, Dry sliding wear of aluminium composites—a review, Comp. Sci. Technol. 57 (1997) 415–435.

[24] B. Venkataraman, G. Sundararajan, Correlation between the characteristics of the mechanically mixed layer and wear behaviour of aluminium Al-7075 alloy and Al-MMCs, Wear 245 (1 and 2) (2000) 22–38.
[25] T.L. Ho, Wear studies on aircraft brake materials, J. Lubr. Technol. 100 (1978) 98–103.
[26] Y.Z. Zhan, G. Zhang, Mechanical mixing and wear-debris formation in the dry sliding wear of copper matrix composite, Tribol. Lett. 17 (3) (2004) 581–592.
[27] S. Wilson, A.T. Alpas, Wear mechanism maps for metal matrix composites, Wear 212 (1997) 41–49.
[28] R.K. Uyyurua, M.K. Surappa, S. Brusethaug, Effect of reinforcement volume fraction and size distribution on the tribological behaviour of Al-composite/brake pad tribo-couple, Wear 260 (2006) 1248–1255.
[29] Y.C. Lin, H.C. Li, S.S. Liou, M.T. Shie, Mechanism of plastic deformation of powder metallurgy metal matrix composites of Cu–Sn/SiC and 6061/SiC under compressive stress, Mater. Sci. Eng. A 373 (2004) 363–369.
[30] A. Farid, S. Guo, On the processing, microstructure, mechanical and wear properties of cermet/stainless steel layer composites, Acta Mater. 55 (2007) 1467–1477.
[31] J. Zechnera, O. Kolednik, Fracture resistance of aluminum multilayer composites, Eng. Fract. Mech. 110 (2013) 489–500.
[32] I.A. Ibrahim, F.A. Mohamed, E.J. Lavernia, Particulate reinforced metal matrix composites—a review, J. Mater. Sci. 26 (1991) 1137–1156.
[33] R.J. Arsenault, S. Fishman, M. Taya, Deformation and fracture behavior of metal–ceramic matrix composite materials, Prog. Mater. Sci. 38 (1994) 1–157.